Qin *et al. Microstructures* 2023;3:2023035
DOI: 10.20517/microstructures.2023.34

Microstructures

Research Article

Open Access

Check for updates

Investigation of $BiFeO_3$-$BaTiO_3$ lead-free piezoelectric ceramics with nonstoichiometric bismuth

Hailan Qin[1,2], Jianwei Zhao[2], Xiaoxin Chen[1,2], Hongtian Li[1,2], Shenghao Wang[2], Yuxiao Du[2], Huanfu Zhou[1], Peifeng Li[2], Dawei Wang[3]

[1]College of Materials Science and Engineering, Guilin University of Technology, Guilin 541004, Guangxi, China.
[2]Shenzhen Institute of Advanced Electronic Materials, Shenzhen Institute of Advanced Technology, Chinese Academy of Sciences, Shenzhen 518055, Guangdong, China.
[3]School of Instrumentation Science and Engineering, Harbin Institute of Technology, Harbin 150080, Heilongjiang, China.

Correspondence to: Prof. Huanfu Zhou, College of Materials Science and Engineering, Guilin University of Technology, Guilin 541004, Guangxi, China. E-mail: zhouhuanfu@163.com; Prof. Peifeng Li, Shenzhen Institute of Advanced Electronic Materials, Shenzhen Institute of Advanced Technology, Chinese Academy of Sciences, Shenzhen 518055, Guangdong, China. E-mail: pf.li1@siat.ac.cn; Prof. Dawei Wang, School of Instrumentation Science and Engineering, Harbin Institute of Technology, Harbin 150080, Heilongjiang, China. E-mail: wangdawei102@gmail.com

How to cite this article: Qin H, Zhao J, Chen X, Li H, Wang S, Du Y, Zhou H, Li P, Wang D. Investigation of $BiFeO_3$-$BaTiO_3$ lead-free piezoelectric ceramics with nonstoichiometric bismuth. *Microstructures* 2023;3:2023035. https://dx.doi.org/10.20517/microstructures.2023.34

Received: 28 Jun 2023 **First Decision:** 1 Aug 2023 **Revised:** 21 Aug 2023 **Accepted:** 25 Aug 2023 **Published:** 19 Sep 2023

Academic Editors: Mojca Otonicar, Xiaozhou Liao **Copy Editor:** Fangyuan Liu **Production Editor:** Fangyuan Liu

Abstract

$BiFeO_3$-$BaTiO_3$ (BF-BT)-based lead-free ceramics are promising piezoelectric materials exhibiting high Curie temperatures and excellent electrochemical properties. In this study, $0.70Bi_{1+x}FeO_3$-$0.30BaTiO_3$ (B_{1+x}F-BT, x = -0.01, 0.00, 0.01, 0.02, 0.03, 0.04) lead-free piezoelectric ceramics were successfully fabricated via the conventional solid-phase reaction process. Crystallographic structure, microstructure, dielectric, impedance, ferroelectric, and piezoelectric properties among different compositions were comprehensively investigated. The X-ray diffraction analysis confirmed that all compositions exhibited a typical perovskite structure with a cubic-rhombohedral phase mixture. The grain size of ceramics tends to increase as the Bi_2O_3 content rises. In particular, the backscattered electron images and energy dispersive analysis revealed prominent core-shell microstructure within grains. Notably, the BF-BT ceramic containing 1% excess Bi displayed the maximum d_{33} ~217 pC/N and d^*_{33} ~243 pm/V accompanied by a high Curie temperature of 515 °C. The findings demonstrate the potential feasibility of BF-BT ceramics in the field of lead-free piezoelectric ceramics.

Keywords: Piezoelectric ceramics, lead-free, BF-BT, bismuth, nonstoichiometric

INTRODUCTION

Piezoelectric ceramics are extensively employed in electronic devices, such as sensors, actuators, filters, ultrasonic devices, *etc.*, which are realized through the mutual conversion between mechanical and electrical energies[1-3]. Over decades, $Pb(Zr_xTi_{1-x})O_3$-based piezoelectric ceramics have been used dominantly in commercial devices. However, the toxicity of lead (Pb) can cause irreversible damage to human health and the environment, which promotes research hotspots on lead-free materials[4-6]. Among the lead-free materials, $(K,Na)NbO_3$ (KNN)-based and $Bi_{1/2}Na_{1/2}TiO_3$ (BNT)-based piezoelectric ceramics are considered to be promising candidates for lead-based piezoelectric ceramics[7-10]. Despite the high piezoelectric coefficient (d_{33} > 500 pC/N), KNN ceramics suffer from certain drawbacks, such as the K and Na volatilization, unstable phase structures near room temperature, and low Curie temperatures (T_C) ~200 °C[1,11-13]. BNT-based ceramics used to exhibit high T_C, but the volatilization of Bi and Na elements leads to unstable chemical compositions and a high coercive field; consequently, superior polarization is difficult to achieve[14-17].

In recent years, $BiFeO_3$-$x$$BaTiO_3$ (BF-xBT) piezoelectric ceramics have emerged as competitive candidates in lead-free materials[2,18-20]. As a kind of multiferroic material, BF has a rhombohedral phase perovskite structure (ABO_3), which has attracted significant attention because of its high T_C (830 °C) and excellent spontaneous polarization (P_s = 90-100 μC/cm²)[21,22]. Recent studies of BF single crystal[23-25], polycrystalline thin film[26-29], and epitaxial thin film[30-34] have also been conducted, which has given researchers additional ideas for exploring and application. However, the synthesis of pure BF is usually accompanied by the generation of impurities, where excess Fe_2O_3 exceeding 5 mol % leads to the formation of pyrochlore $Bi_2Fe_4O_9$ and gamma-Fe_2O_3[35]. Additionally, the volatilization of Bi and the valence reduction of Fe^{3+} to Fe^{2+} at high temperatures cause high leakage currents, resulting in challenges for practical applications[36-38]. BT is a traditional ferroelectric material exhibiting a tetragonal phase structure at room temperature and possesses a low T_C of ~120 °C[39]. It has been found that the sintering of BF-xBT solid solution can effectively suppress the generation of secondary or impurity phases and reduce the leakage current. Specifically, a morphotropic phase boundary (MPB) can be constructed when x approaches 0.30 ~ 0.35, which contributes to enhanced dielectric, piezoelectric, and ferroelectric properties while maintaining a high T_C[40-42].

However, one of the notable disadvantages in BF-xBT-based piezoelectric ceramics is the Bi_2O_3 volatilization during the sintering process, resulting in poor electrical resistivity and piezoelectric performance. The volatilization of Bi_2O_3 can be described by the following defect Equation (1)[43]

$$2Bi^{3+} + 3O^{2-} \rightarrow Bi_2O_3\uparrow + 2V_{Bi}^{3-} + 3V_O^{2+} \quad (1)$$

The volatilization of Bi_2O_3 leads to the generation of Bi vacancies (V_{Bi}^{3-}) and O vacancies (V_O^{2+}) within the ceramics. Various strategies have been attempted to solve the problem. One of the most common strategies is using nonstoichiometric (excess) Bi to compensate for the loss of Bi during high-temperature sintering, as listed in Table 1.

In this study, a series of $0.70B_{1+x}F$-0.30BT (x = -0.01, 0, 0.01, 0.02, 0.03, 0.04) ceramics were fabricated using the conventional solid-state reaction method. The influence of Bi_2O_3 compensation on the phase structure, microstructure, dielectric, ferroelectric, and piezoelectric properties of ceramics are systematically investigated.

Table 1. Summary of ferroelectric and piezoelectric properties of BF-BT system piezoelectric ceramics with excess Bi_2O_3

Composition	d_{33}/ d^*_{33}	P_r (μC/cm²)	T_C (°C)	References
$0.70B_{1.02}F$-0.30BT	183 pC/N	21.38	480	[44]
$0.69B_{1.04}F$-0.31BT	207 pC/N	-	-	[45]
$0.70B_{1.02}F$-0.30BT	211 pm/V	19.6	421	[46]
$0.65B_{1.05}F$-0.35BT	270 pm/V	27.61	432	[47]
$0.70B_{1.02}F$-0.30BT	214 pC/N	19.61	528	[48]
$0.54B_{1.01}F$-0.36BT-0.10BZ	197 pC/N	20	445	[49]
$0.70B_{1.02}$FMT-0.30BT	198 pC/N	-	497	[50]
$0.70B_{1.05}F$-0.30BT	180 pC/N	-	506	[43]
$0.75B_{1.01}F$-0.25BT	114 pC/N	34.4	508	[51]
$0.71B_{1.04}F$-0.29BT	142 pC/N	-	452	[52]

MATERIALS AND METHODS

$0.70Bi_{1+x}FeO_3$-$0.30BaTiO_3$ ($B_{1+x}F$-BT, x = -0.01, 0.00, 0.01, 0.02, 0.03, 0.04) piezoelectric ceramics were fabricated using a solid-state reaction process. Bi_2O_3 (99%, Sinopharm, China), Fe_2O_3 (99.9%, Aladdin, China), $BaCO_3$ (99%, Sinopharm, China), and TiO_2 (98%, Sinopharm, China) powders were employed as raw materials. All powders were weighed according to stoichiometric ratios and ball-milled for 24 h using zirconia balls in ethanol. The mixed slurry was dried and calcined at 750 °C in a sealed alumina crucible for 2 h, followed by a secondary ball-milling process for 12 h. The calcined powder was mixed with a 10 wt% polyvinyl alcohol (PVA) binder, and the green pellets with a diameter of 10 mm were formed under a pressure of 127 MPa. The green pellets were kept at 600 °C for 2 h to burn out PVA and then sintered into ceramics at 1,010 °C for 3 h to obtain ceramics. Silver paste was sintered on parallel ceramic surfaces to form electrodes for electrical measurements.

The crystal structure and morphology were probed by the X-ray powder diffraction (XRD, D8 Advance X, Bruker, Germany) with Cu-K_α radiation and the scanning electron microscope (SEM, Apreo 2, Thermo Scientific, United States) equipped with an energy-dispersive spectroscopy (EDS) detector, respectively. The dielectric and impedance properties were measured via a precision LCR meter (E4980A, Agilent Technologies, United States) connected to a high-temperature dielectric test system (DMS-1000, Balab Technology, China). The ferroelectric hysteresis (*PE*) loops and fieldinduced strain (*SE*) curves were collected by a ferroelectric tester station (PK-10E, PolyK Technologies, United States). The piezoelectric coefficient (d_{33}) is recorded by a quasi-static d_{33} meter (SA1303A, PolyK Technology, United States).

RESULTS AND DISCUSSION

The XRD results reveal that all $B_{1+x}F$-BT compositions exhibit a perovskite structure with a phase mixture consisting of cubic ($Pm\bar{3}m$) and rhombohedral ($R3c$) phases, as shown in Figure 1A. The impurity of $Bi_{25}FeO_{40}$, a common occurrence in the BF-BT system[37], is appeared when $x \geq 0.03$. The enlarged (111) and (200) peaks show insignificant peak shifts with varying Bi_2O_3 content. The refined results for each component are displayed in Figure 1B and Table 2. The cubic phase gradually decreases as the Bi_2O_3 content increases and tends to stabilize at $x \geq 0.01$, according to this Table. This demonstrates that the phase structure changes from the Bi_2O_3-deficient to the Bi_2O_3-excess tends to change from the cubic phase to the rhombohedral phase, while the excess Bi_2O_3 phase structure has little effect, which is also reflected in the lattice parameter.

Table 2. The rietveld refinement data of the observed XRD patterns for B_{1+x}F-BT ceramics

x	Phase fraction (%)		Rhombohedral			Cubic		R_{wp}	χ^2
	Rhombohedral (*R3c*)	Cubic ($Pm\bar{3}m$)	a (Å)	c (Å)	V (Å^3)	a (Å)	V (Å^3)		
-0.01	38	62	5.6454	13.8319	381.781	3.9989	63.948	8.0	1.41
0.00	54	46	5.6437	13.8376	381.704	3.9991	63.958	9.3	1.73
0.01	66	34	5.6393	13.8590	381.689	4.0045	64.281	8.8	1.49
0.02	65	35	5.6396	13.8614	381.805	4.0084	64.407	8.6	1.52
0.03	77	23	5.6389	13.8669	381.854	4.0063	64.303	9.5	1.74
0.04	74	26	5.6389	13.8654	381.812	4.0075	64.363	9.2	1.67

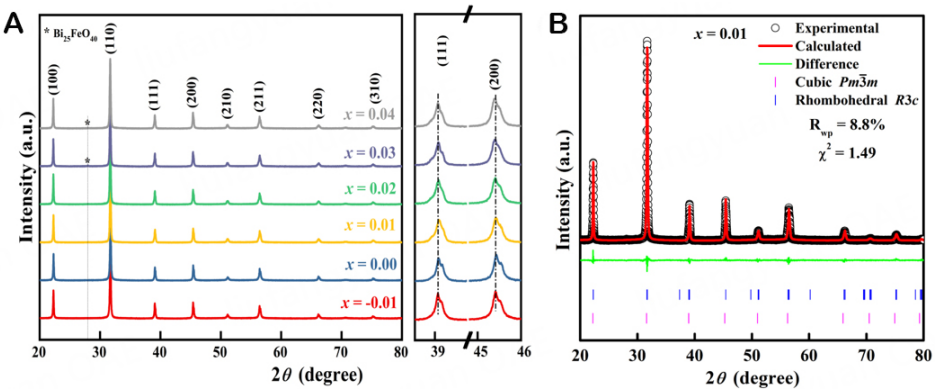

Figure 1. (A) XRD patterns of the B_{1+x}F-BT ceramics, (B) the Rietveld refinement results for x = 0.01.

Figure 2 shows the surface morphology of the B_{1+x}F-BT ceramics in different compositions. The ceramic surface exhibits a compact morphology with clear grain boundaries and seldom pores. The calculated relative density is higher than 95% for all compositions [Supplementary Figure 1], which is consistent with the observations from SEM results. Statistical analysis of the grain size distributions reveals that the grains tend to increase with enriching the Bi_2O_3 content. The ceramic grain size increases from 4.01 μm of x = -0.01 to 9.62 μm of x = 0.04. It is evident that the excess Bi_2O_3 not only compensates for volatilization but also acts as a sintering aid promoting grain growth, which is consistent with the literature[46,47].

Figure 3 shows the backscattered electron (BSE) images of the polished surface of B_{1+x}F-BT ceramics with the corresponding elemental mapping results by EDS. A BSE image is used to see the dark and bright contrast, showing the light and heavy element distributions to evidence the core-shell structure in grains, and EDS helps further identify the exact elements in the core and shell regions. The images reveal a non-uniform distribution of elements inside the ceramic, leading to a distinct core-shell microstructure, which is caused by immiscibility of the dominantly ionically bonded BT and covalently bonded BF phases and the microscopic segregation of elements that forms during the slow cooling process of sintering[3,53-56]. Murakami *et al.* synthesized the $0.05BiScO_3$-$(0.95-x)BaTiO_3$-$xBiFeO_3$ ceramics without a discernible core-shell microstructure[53]; it is proven that the BF-BT lattice can be replaced by dopants in the narrow range of the ionic radius (R_{Sc3+}: 0.745; R_{Ti4+}:0.605; R_{Fe3+}:0.645Å)/electronegativity (E_{Sc3+}:1.3; E_{Ti4+}:1.5; E_{Fe3+}:1.8) difference so as to prevent phase separation during slow cooling processes. Notably, there is a noticeable contrast between light and dark regions in Figure 3. The core, enriched with Bi and Fe, appears brighter, while the shell, enriched with Ba and Ti, appears relatively darker. In addition, the BSE images of x = -0.01 and x = 0.03 and the distribution of EDS elements are shown in Supplementary Figure 2 and Supplementary Figure 3.

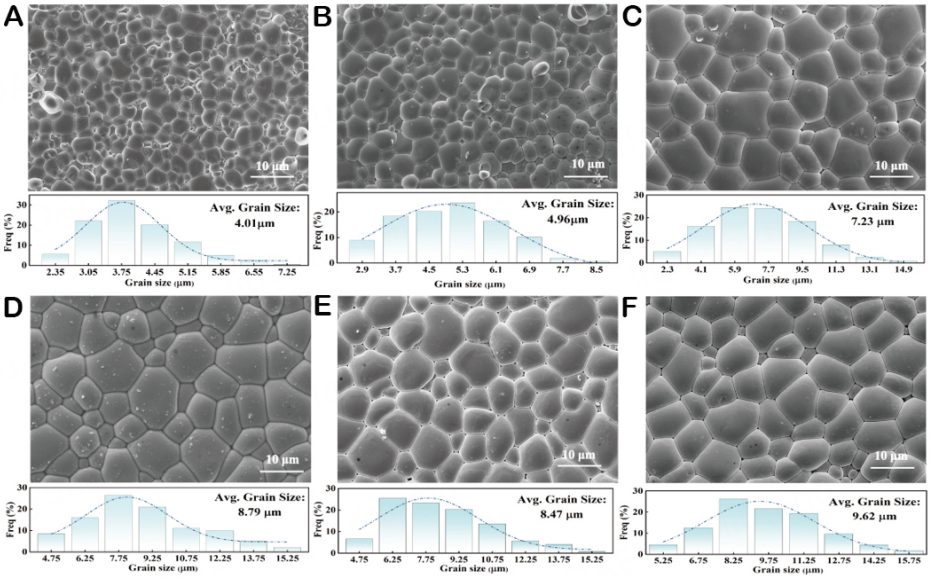

Figure 2. SEM images and grain size distribution in $B_{1+x}F$-BT ceramics with x = (A) -0.01, (B) 0.00, (C) 0.01, (D) 0.02, (E) 0.03, and (F) 0.04.

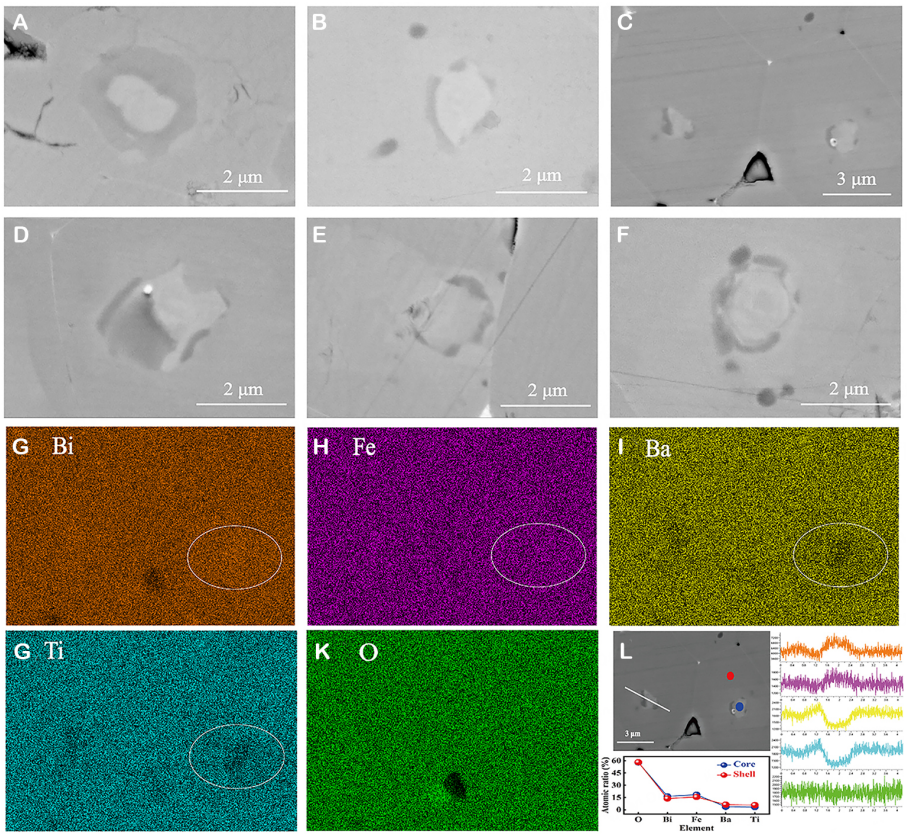

Figure 3. BSE images of $B_{1+x}F$-BT ceramics: x = (A) -0.01, (B) 0.00, (C) 0.01, (D) 0.02, (E) 0.03, (F) 0.04, and EDS elemental mapping results (G) Bi, (H) Fe, (I) Ba, (J) Ti, and (K) O, (L) the scanned points in a core and a shell region and scanned line, EDS data of points and line scan on the core-shell in $B_{1.01}F$-BT ceramic.

Figure 4A presents the temperature-dependent behavior of relative permittivity (ε_r) and dielectric loss (tanδ) at 10 kHz. It reveals that as the Bi_2O_3 content increases, the dielectric peak becomes narrower, and the maximum relative dielectric constant (ε_r) gradually increases, indicating a reduction of diffuse behavior. It is evident from the spectra that the dielectric peaks of the ceramics exhibit asymmetry, which is related to the presence of a core-shell structure within the ceramic grains. As plotted in Figure 4A, the tanδ of ceramics exhibits an abrupt increase around the T_m (temperature exhibiting the maximum ε_r), suggesting that there is a transition from the diffuse ferroelectric to the paraelectric phase [Figure 4B]. Figure 4C illustrates the relaxation factor (γ) calculated at 10 kHz, which demonstrates that the value of γ decreases as the x content increases, ranging from γ = 1.79 at x = -0.01 to γ = 1.27 at x = 0.04. Figure 4D displays the variation of ΔT_m between 1 kHz and 1 MHz for each component in the temperature spectrum. It is evident that ΔT_m tends to decrease with increasing x content, which reveals that the ferroelectricity of the ceramic becomes more prominent, aligning with the decreasing γ depicted in Figure 4C.

The complex impedance (Z^*) plots of B_{1+x}F-BT ceramics at 400 °C are shown in Figure 5A, where Z' and Z'' represent the real part and imaginary part of Z^*, respectively[57]. At 400 °C, the total impedance initially increases from 36.5 kΩ·cm at x = -0.01 to 44.4 kΩ·cm at x = 0.01 and then decreases with incorporating more Bi_2O_3 content, which indicates that the composition of x = 0.01 is the most electrically resistive. The Z'' and M''/ε_0 plots of x = 0.01 at 300 °C are plotted in Figure 5B, illustrating the electrical heterogeneity associated with various conductive components. Three peaks are found in the plots corresponding to the three conductive components. Z'' exhibits a single peak related to the grain boundary response (component 1), while M''/ε_0 shows a strong peak in the low-frequency region and a weak peak in the high-frequency region, which is ascribed to the electrical heterogeneity from the core-shell structure. In this study, the strong peak represents the shell response (component 2), whereas the weaker peak is considered as the core response (component 3). The resistance (R) and capacitance (C) of all conductive components at 325 °C were calculated based on the peaks of Z'' and M''/ε_0 [Table 3]. The R values of components 1 and 2 reach the maximum in the composition of x = 0.01. However, the R value of component 3 did not change significantly with the increase of Bi_2O_3 content. Additionally, the resistance of components 1 and 2 is two orders of magnitude higher than that of component 3, which matches the frequency of the peaks of the three components in Figure 5B. It is worth noting that component 3 exhibits a capacitance that is an order of magnitude higher than components 1 and 2, indicating the formation of an electrically conducting core and a nonconductive shell. Figure 5C shows the Arrhenius plots of the grain shell, core, and boundary, and the calculated activation energy calculated by fitting is shown in Figure 5D. The activation energy of the shell (1.06-1.14 eV) is generally lower than that of the core (1.15-1.28 eV) and grain boundary (1.09-1.16 eV).

Figure 6A illustrates the *PE* loops of the B_{1+x}F-BT ceramics at 60 kV/cm under a frequency of 1 Hz, and the corresponding P_r and E_C are plotted in Figure 6B. The *PE* loops show typical ferroelectric features without observations of leakage characteristics at high field amplitudes. However, when x = -0.01, 0.00, the loops demonstrate the phenomenon of leakage conduction, resulting in relatively high values of P_r and E_C, which is mainly attributed to the formation of Bi and O vacancies caused by the Bi_2O_3 volatilization[43]. When $x \geq 0.01$, the leakage conductivity of BF-BT is significantly reduced, leading to stable values of P_r and E_C. The electric *SE* loops of ceramics measured at 60 kV/cm are shown in Figure 6C. It can be seen that the strain value increases as x increases from -0.01 to 0.01, reaching a maximum value of 0.146% at x = 0.01, and then the strain value decreases. The strains are calculated by averaging the positive strains obtained at ±60 kV/cm and used for deriving the d_{33}^* values, as plotted in Figure 6D. Notably, the highest d_{33}^* = 243 pm/V and d_{33} = 217 pC/N are achieved at x = 0.01, evidencing that the suitable amount of compensation of Bi_2O_3 is effective in improving the piezoelectric properties of the BF-BT ceramics. In addition, the inset image of Figure 6D depicts the temperature dependence of d_{33} for x = 0.01. It demonstrates that the d_{33} value has a

Table 3. The values of *R* and *C* for each component at 325 °C derived based on the *Z*'' and *M*''/ε_0 peak values for -0.01 ≤ *x* ≤ 0.04

Composition	Component 1 (grain boundary)		Component 2 (shell)		Component 3 (core)	
	$R = 2Z''$ (kΩ·cm)	$C = 1/(4\pi f Z'')$ (F cm^{-1})	$R = M''/(\varepsilon_0 \pi f)$ (kΩ·cm)	$C = \varepsilon_0/(2M'')$ (F cm^{-1})	$R = M''/(\varepsilon_0 \pi f)$ (kΩ·cm)	$C = \varepsilon_0/(2M'')$ (F cm^{-1})
-0.01 (325 °C)	346	5.73×10^{-10}	281	4.65×10^{-10}	0.82	1.42×10^{-9}
0.00 (325 °C)	393	6.07×10^{-10}	315	4.77×10^{-10}	1.08	1.30×10^{-9}
0.01 (325 °C)	474	3.48×10^{-10}	378	2.88×10^{-10}	0.95	1.06×10^{-9}
0.02 (325 °C)	438	5.45×10^{-10}	329	4.16×10^{-10}	1.12	1.14×10^{-9}
0.03 (325 °C)	314	5.25×10^{-10}	230	3.93×10^{-10}	0.99	1.08×10^{-9}
0.04 (325 °C)	334	5.41×10^{-10}	245	4.03×10^{-10}	1.07	1.09×10^{-9}

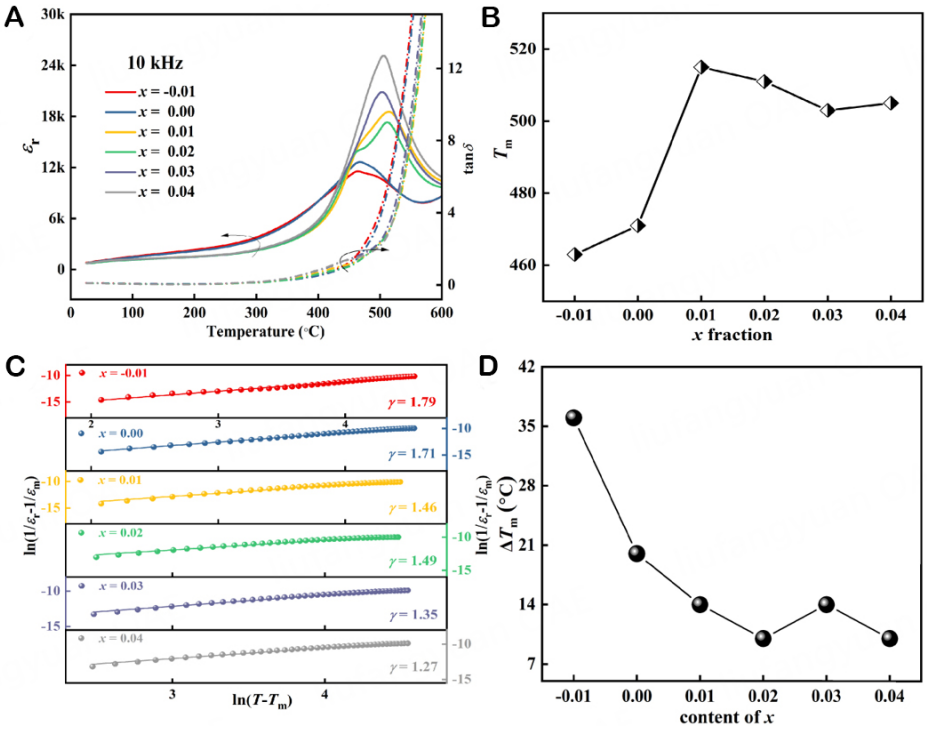

Figure 4. Temperature-dependent ε_r and tanδ of (A) -0.01 ≤ *x* ≤ 0.04 measured at 10 kHz, (B) the T_m at 10 kHz, (C) the relaxation coefficient γ at 10 kHz, (D) the ΔT_m from 1 kHz to 1 MHz for the B_{1+x}F-BT ceramics.

great temperature sensitivity and decreases above 300 °C as a result of the gradual depolarization at high temperatures.

CONCLUSIONS

In this work, a series of $0.70B_{1+x}F$-0.30BT-based lead-free piezoelectric ceramics were systematically studied. The addition of Bi_2O_3 to 0.70BF-BT ceramics plays a crucial role in compensating for the volatilization of Bi elements during high-temperature sintering, leading to enhanced dielectric and piezoelectric performance. The phase structure of the ceramics is barely influenced while varying the Bi_2O_3 content, where all compositions exhibit a typical perovskite structure with a rhombohedral-cubic phase mixture. The microscopy results indicate an increasing trend of grain size as more Bi_2O_3 content is incorporated into the composition. The BSE images and element mappings reveal core-shell microstructures in the ceramics, which are attributed to the segregation of elements during the sintering process. Moreover, the higher Bi_2O_3

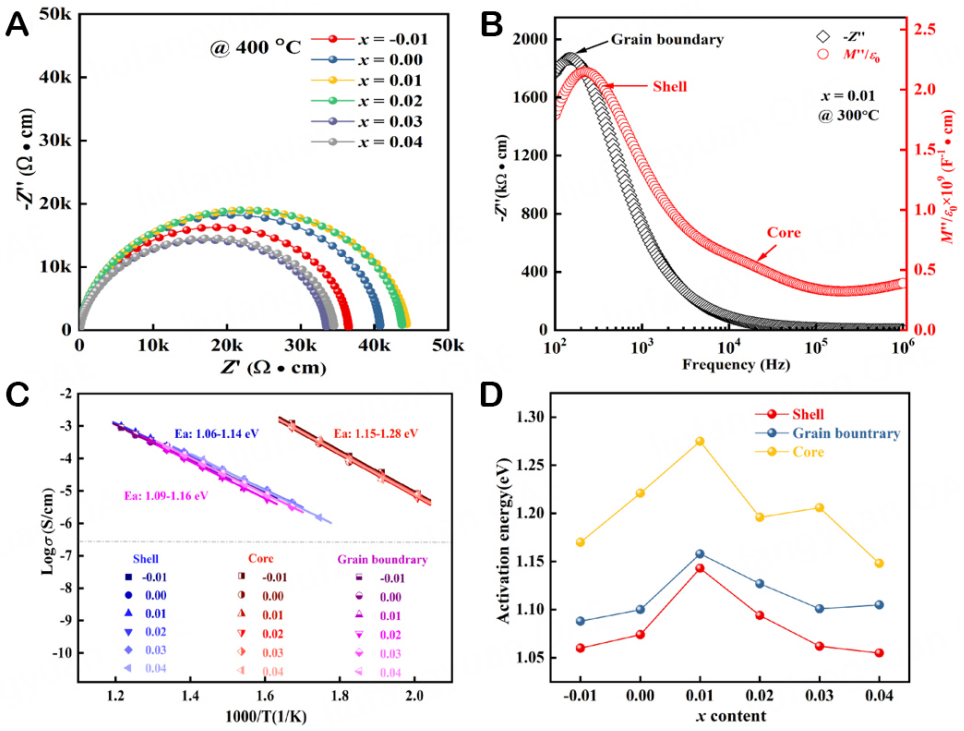

Figure 5. (A)Temperature-dependent Z^* plots for B_{1+x}F-BT ceramics at 400 °C, (B) Combined Z'' and M''/ε_0 spectroscopic plots at 300 °C for x = 0.01, (C) Arrhenius plots and (D) the activation energy for the B_{1+x}F-BT ceramics.

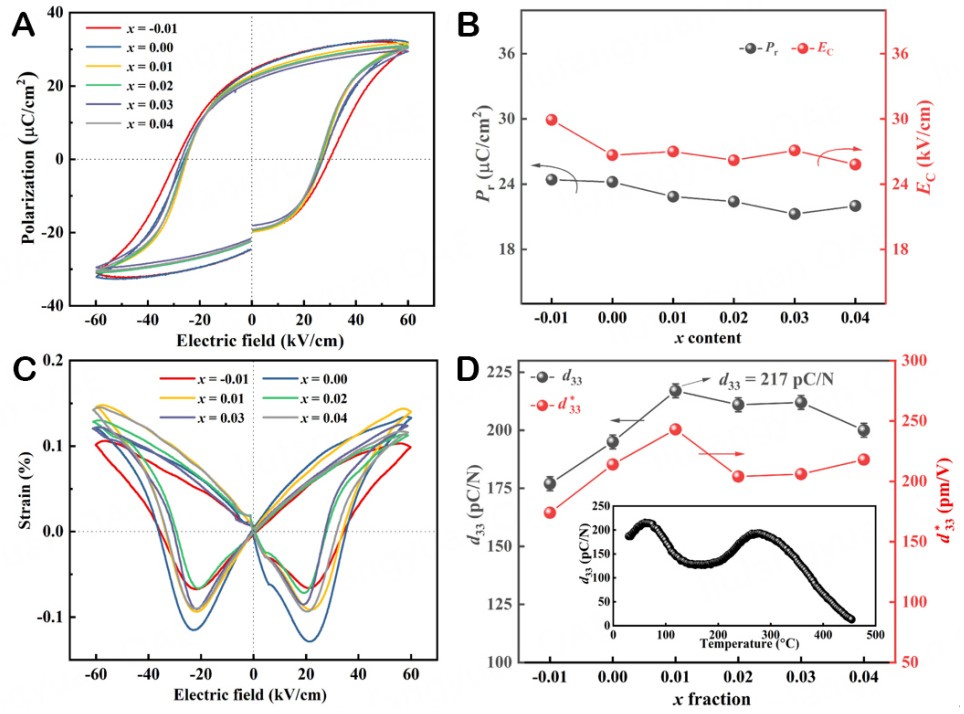

Figure 6. Ferroelectric properties of (A) *PE* loops at 60 kV/cm and associated (B) P_r and E_C of the B_{1+x}F-BT ceramics. (C) *SE* loops at 60 kV/cm and (D) d_{33} and d^*_{33} as a function of x concentration for the B_{1+x}F-BT ceramics; the inset image shows the temperature dependence of d_{33} for x = 0.01.

content leads to narrower dielectric peaks, higher maximum ε_r, and diminished relaxation factor, indicating a deteriorated relaxor behavior. The ferroelectric properties of the ceramics, as demonstrated by *PE* loops, show that the excess of Bi_2O_3 helps improve the leakage conductivity while stabilizing the P_r and E_C. The piezoelectric properties of the ceramics are optimized at $x = 0.01$ with d_{33} ~217 pC/N and d_{33}^* ~243 pm/V, but it has a great temperature sensitivity. The nonstoichiometric optimization of the Bi_2O_3 content in BF-BT was investigated in this work. The findings can be utilized as a foundation for further research into the BF-BT system.

DECLARATIONS

Authors' contributions

Synthesis and testing of materials, data collection, original manuscript writing: Qin H
Validation and original manuscript revision: Zhao J
Data analysis: Chen X, Li H
Data reduction: Wang S
Chart design: Du Y
Validation: Zhou H
Revision: Li P
Reviewing and editing: Wang D

Availability of data and materials

According to reasonable requirements, all of the data examined in this research can be obtained from the correspondents.

Financial support and sponsorship

This work is supported by the Science, Technology and Innovation Committee of Shenzhen Municipality (Grant No. JCYJ20220531095802005 and No. RCBS20210706092341001).

Conflicts of interest

All authors declared that there are no conflicts of interest.

Ethical approval and consent to participate

Not applicable.

Consent for publication

Not applicable.

REFERENCES

1. Saito Y, Takao H, Tani T, et al. Lead-free piezoceramics. *Nature* 2004;432:84-7. DOI
2. Wang D, Wang G, Murakami S, et al. $BiFeO_3$-$BaTiO_3$: a new generation of lead-free electroceramics. *J Adv Dielect* 2018;8:1830004. DOI
3. Murakami S, Wang D, Mostaed A, et al. High strain (0.4%) $Bi(Mg_{2/3}Nb_{1/3})O_3$-$BaTiO_3$-$BiFeO_3$ lead-free piezoelectric ceramics and multilayers. *J Am Ceram Soc* 2018;101:5428-42. DOI
4. Panda PK, Sahoo B. PZT to Lead Free Piezo Ceramics: a review. *Ferroelectrics* 2015;474:128-43. DOI
5. Souza-Araujo J, Hussey NE, Hauser-Davis RA, Rosa AH, Lima MO, Giarrizzo T. Human risk assessment of toxic elements (As, Cd, Hg, Pb) in marine fish from the Amazon. *Chemosphere* 2022;301:134575. DOI PubMed
6. McFarland MJ, Hauer ME, Reuben A. Half of US population exposed to adverse lead levels in early childhood. *Proc Natl Acad Sci*

USA 2022;119:e2118631119. DOI PubMed PMC
7. Liu K, Zhang Y, Marwat MA, et al. Large electrostrain in low-temperature sintered NBT-BT-0.025FN incipient piezoceramics. *J Am Ceram Soc* 2020;103:3739-47. DOI
8. Zhang Y, Liu X, Wang G, et al. Enhanced mechanical energy harvesting capability in sodium bismuth titanate based lead-free piezoelectric. *J Alloys Compd* 2020;825:154020. DOI
9. Wang D, Hussain F, Khesro A, et al. Composition and temperature dependence of structure and piezoelectricity in (1-x)($K_{1-y}Na_y$)NbO_3 -x($Bi_{1/2}Na_{1/2}$)ZrO_3 lead-free ceramics. *J Am Ceram Soc* 2017;100:627-37. DOI
10. Khesro A, Wang D, Hussain F, et al. Temperature dependent piezoelectric properties of lead-free (1-*x*)$K_{0.6}Na_{0.4}NbO_3$-*x*$BiFeO_3$ ceramics. *Front Mater* 2020;7:140. DOI
11. Zhang S, Kounga AB, Aulbach E, Ehrenberg H, Rödel J. Giant strain in lead-free piezoceramics $Bi_{0.5}Na_{0.5}TiO_3$-$BaTiO_3$-$K_{0.5}Na_{0.5}NbO_3$ system. *Appl Phys Lett* 2007;91:112906. DOI
12. Zheng T, Wu J, Xiao D, Zhu J. Giant d_{33} in nonstoichiometric (K,Na)NbO_3-based lead-free ceramics. *Scr Mater* 2015;94:25-7. DOI
13. Shi H, Chen J, Wang R, Dong S. Full set of material constants of ($Na_{0.5}K_{0.5}$)NbO_3-$BaZrO_3$-($Bi_{0.5}Li_{0.5}$)TiO_3 lead-free piezoelectric ceramics at the morphotropic phase boundary. *J Alloys Compd* 2016;655:290-5. DOI
14. Bai W, Li P, Li L, Zhang J, Shen B, Zhai J. Structure evolution and large strain response in BNT-BT lead-free piezoceramics modified with $Bi(Ni_{0.5}Ti_{0.5})O_3$. *J Alloys Compd* 2015;649:772-81. DOI
15. Hiruma Y, Nagata H, Takenaka T. Formation of morphotropic phase boundary and electrical properties of ($Bi_{1/2}Na_{1/2}$)TiO_3-$Ba(Al_{1/2}Nb_{1/2})O_3$ solid solution ceramics. *Jpn J Appl Phys* 2009;48:09KC08. DOI
16. Dittmer R, Webber KG, Aulbach E, Jo W, Tan X, Rödel J. Electric-field-induced polarization and strain in 0.94($Bi_{1/2}Na_{1/2}$)TiO_3-0.06$BaTiO_3$ under uniaxial stress. *Acta Mater* 2013;61:1350-8. DOI
17. Li T, Lou X, Ke X, et al. Giant strain with low hysteresis in A-site-deficient ($Bi_{0.5}Na_{0.5}$)TiO_3-based lead-free piezoceramics. *Acta Mater* 2017;128:337-44. DOI
18. Wang G, Hu T, Zhu W, et al. Multiple local symmetries result in a common average polar axis in high-strain $BiFeO_3$-based ceramics. *Phys Rev Lett* 2023;130:076801. DOI
19. Lu Z, Wang G, Li L, et al. In situ poling X-ray diffraction studies of lead-free $BiFeO_3$-$SrTiO_3$ ceramics. *Mater Today Phys* 2021;19:100426. DOI
20. Wang G, Fan Z, Murakami S, et al. Origin of the large electrostrain in $BiFeO_3$-$BaTiO_3$ based lead-free ceramics. *J Mater Chem A* 2019;7:21254-63. DOI
21. Li Z, Hou Z, Song W, et al. Mg-substitution for promoting magnetic and ferroelectric properties of $BiFeO_3$ multiferroic nanoparticles. *Mater Lett* 2016;175:207-11. DOI
22. Wang D, Wang M, Liu F, et al. Sol-gel synthesis of Nd-doped $BiFeO_3$ multiferroic and its characterization. *Ceram Int* 2015;41:8768-72. DOI
23. Sono N, Kinoshita Y, Kida N, Ito T, Okamoto H, Miyamoto T. Terahertz-field-induced changes of electronic states associated with a polarization modulation in $BiFeO_3$. *J Phys Soc Jpn* 2021;90:033703. DOI
24. Huang S, Hong F, Xia Z, et al. Multiferroic behavior from synergetic response of multiple ordering parameters in $BiFeO_3$ single crystal under high magnetic field up to 50 tesla. *J Appl Phys* 2020;127:044101. DOI
25. Białek M, Ito T, Rønnow H, Ansermet J. Terahertz-optical properties of a bismuth ferrite single crystal. *Phys Rev B* 2019;99:064429. DOI
26. Blázquez Martínez A, Grysan P, Girod S, et al. Strain engineering of the electro-optic effect in polycrystalline $BiFeO_3$ films [invited]. *Opt Mater Express* 2023;13:2061-70. DOI
27. Yi J, Liu L, Shu L, Huang Y, Li JF. Outstanding ferroelectricity in Sol-gel-derived polycrystalline $BiFeO_3$ films within a wide thickness range. *ACS Appl Mater Interfaces* 2022;14:21696-704. DOI
28. Zhou Y, Wang C, Tian S, et al. Switchable ferroelectric diode and photovoltaic effects in polycrystalline $BiFeO_3$ thin films grown on transparent substrates. *Thin Solid Films* 2020;698:137851. DOI
29. Önal F, Maksutoglu M, Zarbali M, Mikailzade F. Magnetization and magnetic resonance in sol-gel derived polycrystalline $BiFeO_3$ film. *J Magn Magn Mater* 2019;477:92-8. DOI
30. Song H, Son JY. Physical properties of Cr-doped epitaxial $BiFeO_3$ thin films influenced by ferroelectric domain structures. *J Phys Chem Solids* 2023;177:111306. DOI
31. Ding J, Guo R, Hu J, et al. Switchable ferroelectric photovoltaic in the low bandgap cobalt-substituted $BiFeO_3$ epitaxial thin films. *Appl Surf Sci* 2022;606:154898. DOI
32. Lee JY, Anoop G, Unithrattil S, et al. The role of intermediate S-polymorph towards high piezoelectricity in La-doped $BiFeO_3$ epitaxial thin films. *Acta Mater* 2021;207:116683. DOI
33. Pei W, Chen J, You D, et al. Enhanced photovoltaic effect in Ca and Mn co-doped $BiFeO_3$ epitaxial thin films. *Appl Surf Sci* 2020;530:147194. DOI
34. Zhou Z, Sun W, Liao Z, Ning S, Zhu J, Li J. Ferroelectric domains and phase transition of sol-gel processed epitaxial Sm-doped $BiFeO_3$ (001) thin films. *J Mater* 2018;4:27-34. DOI
35. Lahmar A, Zhao K, Habouti S, Dietze M, Solterbeck C, Es-souni M. Off-stoichiometry effects on $BiFeO_3$ thin films. *Solid State Ionics* 2011;202:1-5. DOI
36. Wang J, Neaton JB, Zheng H, et al. Epitaxial $BiFeO_3$ multiferroic thin film heterostructures. *Science* 2003;299:1719-22. DOI
37. Rojac T, Bencan A, Malic B, et al. $BiFeO_3$ ceramics: processing, electrical, and electromechanical properties. *J Am Ceram Soc*

2014;97:1993-2011. DOI

38. Rojac T, Kosec M, Budic B, Setter N, Damjanovic D. Strong ferroelectric domain-wall pinning in $BiFeO_3$ ceramics. *J Appl Phys* 2010;108:074107. DOI
39. Ismailzade IH, Ismailov RM, Alekberov AI, Salaev FM. Investigation of the magnetoelectric $(ME)_H$ effect in solid solutions of the systems $BiFeO_3$-$BaTiO_3$ and $BiFeO_3$-$PbTiO_3$. *Phys Status Solid* 1981;68:K81-5. DOI
40. Wei Y, Wang X, Zhu J, Wang X, Jia J, Damjanovic D. Dielectric, ferroelectric, and piezoelectric properties of $BiFeO_3$-$BaTiO_3$ ceramics. *J Am Ceram Soc* 2013;96:3163-8. DOI
41. Habib M, Lee MH, Kim DJ, et al. Phase evolution and origin of the high piezoelectric properties in lead-free $BiFeO_3$-$BaTiO_3$ ceramics. *Ceram Int* 2020;46:22239-52. DOI
42. Kumar MM, Srinivas A, Suryanarayana SV. Structure property relations in $BiFeO_3$/$BaTiO_3$ solid solutions. *J Appl Phys* 2000;87:855-62. DOI
43. Zheng T, Ding Y, Wu J. Bi nonstoichiometry and composition engineering in (1-*x*)$Bi_{1+y}FeO_{3+3y/2}$-*x*$BaTiO_3$ ceramics. *RSC Adv* 2016;6:90831-9. DOI
44. Yang L, Chen C, Jiang X, Huang X, Nie X, Chang S. Enhanced ferroelectric and piezoelectric properties of $BiFeO_3$-$BaTiO_3$ lead-free ceramics by simultaneous optimization of Bi compensation and sintering conditions. *Ceram Int* 2022;48:12866-74. DOI
45. Yi W, Lu Z, Liu X, et al. Excellent piezoelectric performance of Bi-compensated 0.69$BiFeO_3$-0.31$BaTiO_3$ lead-free piezoceramics. *J Mater Sci Mater Electron* 2021;32:22637-44. DOI
46. Zhang G, Dai J, Lu Y. Phase structure and electrical properties of (1-*x*)$Bi_{1+y}FeO_3$-*x*$BaTiO_3$ lead-free ceramics with different Bi contents. *J Mater Sci Mater Electron* 2021;32:10289-98. DOI
47. Ahmed T, Khan SA, Bae J, et al. Role of Bi chemical pressure on electrical properties of $BiFeO_3$-$BaTiO_3$-based ceramics. *Solid State Sci* 2021;114:106562. DOI
48. Xun B, Wang N, Zhang B, et al. Enhanced piezoelectric properties of 0.7$BiFeO_3$-0.3$BaTiO_3$ lead-free piezoceramics with high Curie temperature by optimizing Bi self-compensation. *Ceram Int* 2019;45:24382-91. DOI
49. Jian J, Peng R, Fu D, Chen J, Cheng J. Structure and enhanced electrical properties of high-temperature $BiFeO_3$-$PbTiO_3$-$BaZrO_3$ ceramics with bismuth excess. *Ceram Int* 2018;44:21774-8. DOI
50. Zhu L, Zhang B, Li S, Zhao G. Large piezoelectric responses of Bi(Fe,Mg,Ti)O_3-$BaTiO_3$ lead-free piezoceramics near the morphotropic phase boundary. *J Alloys Compd* 2017;727:382-9. DOI
51. Chen J, Cheng J. Enhanced thermal stability of lead-free high temperature 0.75$BiFeO_3$-0.25$BaTiO_3$ ceramics with excess Bi content. *J Alloys Compd* 2014;589:115-9. DOI
52. Zhou C, Yang H, Zhou Q, Chen G, Li W, Wang H. Effects of Bi excess on the structure and electrical properties of high-temperature $BiFeO_3$-$BaTiO_3$ piezoelectric ceramics. *J Mater Sci Mater Electron* 2013;24:1685-9. DOI
53. Murakami S, Ahmed NTAF, Wang D, Feteira A, Sinclair DC, Reaney IM. Optimising dopants and properties in $BiMeO_3$ (Me = Al, Ga, Sc, Y, $Mg_{2/3}Nb_{1/3}$, $Zn_{2/3}Nb_{1/3}$, $Zn_{1/2}Ti_{1/2}$) lead-free $BaTiO_3$-$BiFeO_3$ based ceramics for actuator applications. *J Eur Ceram Soc* 2018;38:4220-31. DOI
54. Calisir I, Hall DA. Chemical heterogeneity and approaches to its control in $BiFeO_3$-$BaTiO_3$ lead-free ferroelectrics. *J Mater Chem C* 2018;6:134-46. DOI
55. Wang D, Fan Z, Li W, et al. High energy storage density and large strain in Bi($Zn_{2/3}Nb_{1/3}$)O_3-doped $BiFeO_3$-$BaTiO_3$ ceramics. *ACS Appl Energy Mater* 2018;1:4403-12. DOI
56. Calisir I, Amirov AA, Kleppe AK, Hall DA. Optimisation of functional properties in lead-free $BiFeO_3$-$BaTiO_3$ ceramics through La^{3+} substitution strategy. *J Mater Chem A* 2018;6:5378-97. DOI
57. Lu Z, Wang G, Bao W, et al. Superior energy density through tailored dopant strategies in multilayer ceramic capacitors. *Energy Environ Sci* 2020;13:2938-48. DOI